



Contents lists available at ScienceDirect

Remote Sensing Applications: Society and Environment

journal homepage: www.elsevier.com/locate/rsase



Integrating high-resolution imagery, deep learning, and GIS to estimate soil erosion following timber harvesting

Manisha Parajuli ^{a,b,*}, Richard Cristan ^b, Marissa Jo Daniel ^b, Arjun Rijal ^b, Dana Mitchell ^c, Timothy McDonald ^d, Tom Gallagher ^b

^a College of Agriculture, Health, & Natural Resources, Kentucky State University, Frankfort, KY, 40601, USA

^b College of Forestry, Wildlife and Environment, Auburn University, Auburn, AL, 36849, USA

^c Department of Energy, Bioenergy Technologies Office, USA

^d Department of Biosystems Engineering, Auburn University, Auburn, AL, 36849, USA



ARTICLE INFO

Keywords:

Forest operations
Forest management
Forestry best management practices
Semantic segmentation
UAV

ABSTRACT

Conventionally, soil erosion estimation has depended on ground-based methods; however, remote sensing offers a promising alternative for erosion estimation across various land uses and land cover classes (LULC). Determining erosion potential of a harvest site, considering different harvest categories, requires accurate segmentation of each category. In this study, we encompassed 20 harvest sites in the southeastern United States and utilized high-resolution imagery from unmanned aerial vehicle (UAV), geographic information system (GIS) data, and deep learning models to segment various harvest categories within each site and estimate soil erosion potential. Site data used to predict erosion included rainfall and runoff erosivity factor (R), soil erodibility factor (K), slope-length factor (L), slope-steepness factor (S), cover and management factor (C), and support practice factor (P). Six models based on U-Net, Deeplab V3, and PSPNet architectures, utilizing ResNet-34 and ResNet-50 backbones, were trained and evaluated for their accuracy in segmenting harvest categories. The model trained with Deeplab V3 architecture and ResNet-34 backbone demonstrated superior precision, recall, and F1 values compared to the others and was selected for segmenting the orthomosaic maps of the harvest sites into different harvest categories. Subsequently, using the classified orthomosaic and field-based data, a CP raster layer of each harvest site was prepared. The study revealed that roads exhibit the highest potential erosion rate, followed by skid trails, loading decks, clear-cut areas, clear-cut areas with vegetation, and streamside management zones (SMZs). The overall average erosion rate from all the harvest sites was 0.78 tonnes per hectare annually. Furthermore, the documented CP factor provides a time-efficient alternative for soil erosion estimation, reducing reliance on field-intensive on-site assessments. Overall, this study demonstrates how integrating these advanced technologies provides a reliable and efficient approach to assess soil erosion potential at harvest sites.

1. Introduction

Forests in the southern United States (US) are typically intensively managed (timber harvesting, site preparation, and reforestation)

* Corresponding author. College of Agriculture, Health, & Natural Resources, Kentucky State University, Frankfort, KY, 40601, USA.
E-mail address: manisha.parajuli@kysu.edu (M. Parajuli).

<https://doi.org/10.1016/j.rsase.2025.101498>

Received 8 November 2024; Received in revised form 7 February 2025; Accepted 20 February 2025

Available online 25 February 2025

2352-9385/© 2025 The Authors. Published by Elsevier B.V. This is an open access article under the CC BY-NC license (<http://creativecommons.org/licenses/by-nc/4.0/>).

and require the use of heavy machinery, which is similar to other regions of the US with the use of heavy machinery for harvesting timber (Hiesl and Benjamin, 2013; Murray et al., 2023; Parajuli, 2021; Soman et al., 2020). When best management practices (BMPs) are not properly implemented, these activities can negatively impact forest soil (Cristan et al., 2016; Hawks et al., 2022; Parajuli et al., 2024). Although soil erosion is a natural phenomenon, timber harvesting without proper BMP implementation can accelerate soil erosion and sedimentation, leading to degraded water quality. Harvesting activities combined with rainfall and site characteristics can cause varying degrees of soil erosion and sedimentation, which can impair water quality by reducing stream depth, increasing turbidity, elevating nutrient pollution, and disrupting aquatic habitats (Binkley and Brown, 1993; Cristan et al., 2016; Hawks et al., 2022). Erosion processes exhibit significant temporal and spatial dynamics, making it crucial to understand and map these processes in detail over time and space (Samarin et al., 2020; Shruthi et al., 2015). It is essential to monitor soil erosion on timber harvests to understand the current soil erosion status and prepare effective management plans. By estimating soil erosion potential and identifying critical areas immediately after harvesting, forest managers can better plan post-harvesting management activities and implement BMPs according to the site conditions.

Various methods can be used for estimating erosion, including conventional on-the-ground surveys (hereafter referred to as 'conventional survey') using the Universal Soil Loss Equation (USLE) forest handbook (hereafter referred to as 'USLE handbook'), remote sensing and Geographic Information System (GIS) approaches, Revised USLE 2 (RUSLE 2), and the web-based Water Erosion Prediction Project (WEPP). Remote sensing and GIS, RUSLE 2, and WEPP tools are viable computer-based alternatives (Laflen et al., 1997; McCool et al., 2004).

In the US, soil erosion estimation began in the early 1900s. In the 1940's, AW. Zingg introduced the first mathematical equation to estimate soil erosion losses (Cooper, 2011; Zingg, 1940). Walt Wischmeier and Dwight Smith introduced the USLE in 1965 and a revised version in 1978 which had improvements made to the variables and a westward expansion (Wischmeier and Smith, 1978). Several research works have modified USLE's factors for local and regional conditions (Duarte et al., 2021; Li et al., 2024; Moody, 2020; Panagos et al., 2012; Pinson and AuBuchon, 2023; Renard and Freimund, 1994). Originally designed for agricultural purposes, USLE has been adapted to more accurately predict sheet and rill erosion on forest lands. It estimates erosion in areas where forest management activities or other operations expose soil to the erosive forces of rainfall and runoff (Renard, 1997; Renard and Freimund, 1994).

Conventional survey for soil erosion estimation can be time-intensive and labor-intensive, requiring meticulous fieldwork while navigating challenges like terrain, site wetness, and harvest site scale (Parajuli et al., 2024; Rijal et al., 2023). With the advancements in technology, integrating USLE with remote sensing and GIS is becoming popular for soil erosion estimation; offering enhanced estimation accuracy and spatial distribution at reasonable costs (Duarte et al., 2021; Moody, 2020; Rawat et al., 2016; Zerihun et al., 2018). It also provides visualization and faster analysis of erosion potential and allows simulation of large-scale studies using large amounts of data requiring a relatively short processing time (Blaszczyński, 2001). Parameters such as slope and aspect, derived from Digital Elevation Model (DEM) and Land Use Land Cover (LULC) information, can be easily integrated with the USLE using GIS tools (Ganasri and Ramesh, 2016; Malinowski et al., 2023). Many studies have integrated remote sensing, GIS, and the USLE to estimate soil erosion potential across large LULC categories, incorporating various cover classes such as forests, barren lands, water bodies, agricultural land, and buildings (Farhan and Nawaiseh, 2015; Ganasri and Ramesh, 2016; Kim and Maidment, 2014). However, these studies often treated entire forests as a single land use category, assigning a uniform value for forest areas. Harvested forests, however, include distinct categories such as forest roads, skid trails, loading decks, Streamside Management Zones (SMZs), and clear-cut areas (excluding roads, skid trails, loading decks, stream crossings, and SMZs). Each category has unique functions, operational needs, and varying rates of soil erosion due to different levels of disturbance (Barrett et al., 2016; Hawks et al., 2022). There is a need for research to develop a comprehensive framework integrating GIS, remote sensing, and USLE for harvest sites to account for varying erosion potentials of different harvest categories and provide more precise soil erosion assessments. Furthermore, information on CP values for each forest harvest category is not yet available for reference. Therefore, this study aims to document the CP values for various harvest categories across the study sites, providing valuable data to support future research and applications.

Integrating high-resolution Unmanned Aerial Vehicle (UAV) imagery with deep learning algorithms has demonstrated significant potential to reliably map, detect features, classify, and segment objects (Bouguettaya et al., 2022; Pearse et al., 2020). Various deep learning models, including U-Net, DeepLab V3, and Pyramid Scene Parsing Network (PSPNet), are widely used in remote sensing for segmentation tasks, classification, and feature detection tasks (Jeppesen et al., 2019; Sun et al., 2023). For instance, a study by Jeppesen et al. (2019) used U-Net to detect clouds in optical satellite imagery in Denmark. Guo et al. (2022) utilized models such as ResNet, DenseNet, and GoogleNet to improve the classification accuracy of individual tree species in China. Similarly, Yang et al. (2022) explored the effectiveness of Convolutional Neural Networks (CNN) in detecting and mapping tree crowns within the highly diverse urban forest of New York's Central Park. Sun et al. (2023) evaluated the performance of four semantic segmentation models (U-Net, DeepLab V3, PSPNet, and DeepLab V3+) to detect chestnut (*Castanea mollissima* Blume) cover areas in China. These deep learning techniques have revolutionized remote sensing, particularly in image classification, due to their ability to automate feature extraction and processing, ensuring high accuracy and efficiency in analyzing and interpreting complex imagery data (Ma et al., 2019; Yuan et al., 2020). This advancement holds significant implications for fields such as geomorphology, hydrology, and environmental management, where detailed terrain models are crucial for watershed studies, erosion assessments, disaster risk analysis, and land use planning (Althoff et al., 2021; Khosravi et al., 2023; Ma and Mei, 2021). Although these techniques are commonly applied across various disciplines, their potential applications in segmenting a harvest site into different harvest categories and estimating soil erosion remain largely unexplored.

This research aims to assess soil erosion risk at timber harvest sites in the southeastern US by integrating USLE, high-resolution imagery, GIS, and deep learning algorithms. The primary objective is to train deep learning models with pre-trained architectures

and backbone networks to segment different harvest categories. This will identify areas at high risk of soil erosion that require effective management strategies. Additionally, the study aims to develop a comprehensive framework for soil erosion assessments using these advanced tools and documenting CP values for various harvest site categories. The innovative aspect of this methodology lies in utilizing high-resolution imagery and deep learning for precise operational feature segmentation, offering valuable contributions to environmental management and forest conservation by providing new insights into managing soil erosion risks in timber harvest sites.

2. Materials and methods

2.1. Study area

The study covers 20 harvest sites located within the Coastal Plain region of the southeastern US: Alabama ($n = 10$), Georgia ($n = 5$), and Florida ($n = 5$) (Fig. 1). The most common harvest system available in this region is whole tree harvesting which includes using equipment such as a feller buncher, grapple skidder, and loader. The common type of soil in the Coastal Plain of Alabama is sandy topsoil and clayey subsoil (McWilliams, 1992). Similarly, soil in the Coastal Plain of Georgia is predominantly sandy and loamy and Florida features a wide range of soil types, from sandy soils in the uplands to more organic, peaty soils in lower-lying areas near water bodies (Watts and Collins, 2008). The selected sites were harvested within one year of field data collection in the summer of 2022.

Each study site was surveyed using a commercially available, consumer-grade rotary-wing UAV, commonly used by foresters and loggers. This UAV was equipped with a Global Positioning System (GPS) and an Inertial Measurement Unit (IMU) for precise navigation and control. It also featured an integrated Red, Green, and Blue (RGB) camera to capture georeferenced imagery and videos. The UAV surveys were pre-planned and conducted automatically via the Dronelink app (<https://www.dronelink.com/>). Flight parameters included a 70% forward overlap and a 70% sidelap at an altitude of 91.44 m (300 feet) above ground level, with a flight speed of 8 m per second. Orthomosaic maps for each study site were generated using ArcGIS Drone2Map (Esri, 2022). We evaluated six harvest operational categories within the forest (where applicable to the site) to estimate erosion on each harvest site: roads, skid trails, SMZs, loading decks, clear cut (CC), and CC with vegetation (Fig. 2).

In addition to UAV surveys, we conducted conventional surveys to estimate and validate soil erosion rates at each harvest site. The USLE approach was adapted for forestland using the guidelines provided in the handbook by Dissmeyer and Foster (1984). The USLE equation for estimating soil loss is:

$$A = R \times K \times L^*S \times C^*P \quad \text{Equation (1)}$$

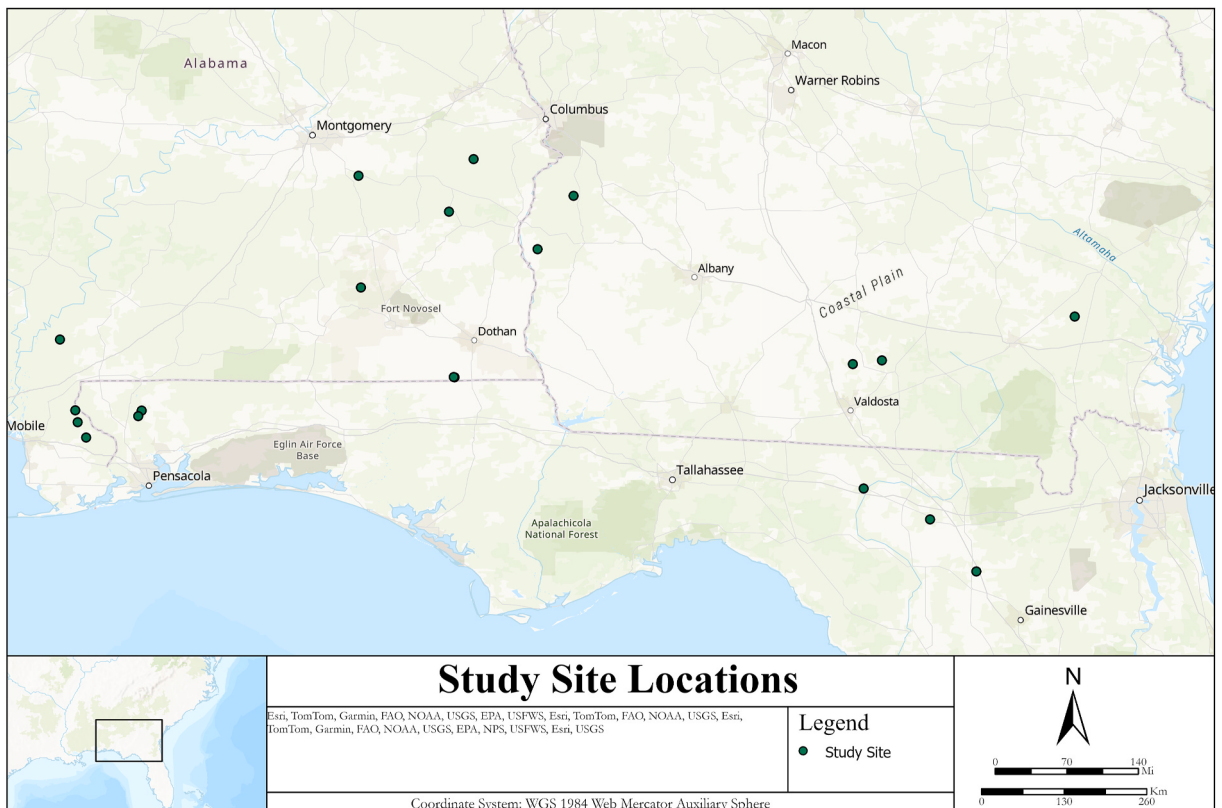


Fig. 1. Map of the study area.

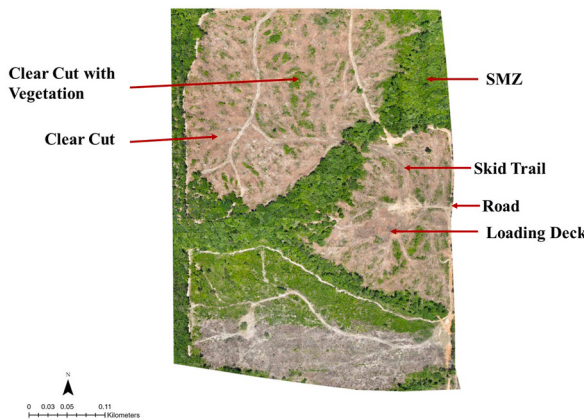


Fig. 2. Orthomosaic image of a harvest site illustrating various harvest categories.

Where, A is soil loss per unit area, tons/acre/year (tonnes/hectare/year or t/ha/yr), R is rainfall and runoff erosivity factor, K is soil erodibility factor, L is slope-length factor, S is slope-steepness factor, C is cover and management factor, and P is support practice factor.

The findings from the field-based study have been previously published, with the detailed methodology outlined in [Parajuli et al. \(2024\)](#).

2.2. Data sources and analysis

2.2.1. R factor

Rainfall data were obtained from the National Oceanic and Atmospheric Administration (NOAA). For each site, rainfall data spanning the past 20 years were downloaded, representing data collected from rain gauge stations located in the respective counties. This data was used to estimate the spatial distribution of average annual precipitation (P) in the study area through the 'Kriging' method of interpolation ([Ganasri and Ramesh, 2016](#)). Using the raster calculator function in ArcGIS Pro 3.2 software, the mean annual precipitation was converted into a raster layer of R factor with a resolution of 0.5 m (meters). [Renard and Freimund \(1994\)](#) equations were used to derive the R factor from the average annual precipitation (mm), for the conterminous US. When average annual precipitation was less than 850 mm, Equation (2) was applied. For average annual precipitation greater than or equal to 850 mm, Equation (3) was applied:

$$R = 0.04830 P^{1.610} \quad \text{Equation (2)}$$

$$R = 587.8 - 1.219P + 0.004105 P^2 \quad \text{Equation (3)}$$

Where, R is rainfall and runoff erosivity factor (MJ·mm/ha·hr·yr.) and P is average annual precipitation (mm).

2.2.2. K factor

The ArcGIS Soil Survey Geographic Database (SSURGO) was used to obtain K-factor data for our study sites ([Web Soil Survey, 2019](#)). These data were imported into ArcGIS Pro 3.2 and converted into a K-factor raster layer with a resolution of 0.5 m.

2.2.3. L and S factors

DEM for each site was created using Light Detection and Ranging (LiDAR) point cloud data obtained from the United States Geological Survey's 3D Elevation Program (USGS 3DEP) and NOAA, which was accessed via OpenTopography. The data underwent initial processing in ArcGIS Pro 3.2 to classify ground points and the classified points were then used to generate DEMs at a 0.5 m resolution. These DEMs were then used to calculate slope-length and steepness using the Grid Cumulation (GC) method and the Maximum Downhill Slope (MDS) approach ([Moody, 2020](#)).

Using the GC method, slope-length was calculated based on the flow path length. High-resolution DEMs were utilized to provide precise slope angle estimates that accurately reflect the true topography of the landscape. During the analysis, DEM was evaluated using a pre-determined cut-off slope angle, which serves as the minimum slope angle necessary for erosion calculations. Flow direction over the landscape was derived from the DEM to identify the likely paths water would take as it descends the slopes, thus influencing erosion patterns. The flow direction data was then used to determine the non-cumulative slope-length, which is the distance water travels before reaching a steady state of flow. For regions with a zero slope angle (flat areas), a value of 0.1 was assigned to account for slight inclines that might not be detected by the DEM, recognizing that completely flat areas are rare ([Moody, 2020](#)). High points, where all flow paths originate, were identified as cells with no neighboring cells having corresponding flow directions, based on the D8 flow routing algorithm. Cumulative slope-length calculations were terminated when two flow paths converged (with the shorter path

ending), when a stream channel was encountered, or when the slope angle decreased sufficiently for deposition to occur. The total slope-length, contributing to the 'L' factor, was calculated by cumulatively adding the slope-lengths from the identified starting points along the flow path. Adjustments were made for any slope-lengths exceeding the cutoff slope angle to refine the cumulative slope-length values.

The method for calculating the L factor is presented in Fig. 3.

The slope-steepness was determined using the MDS method (Dunn and Hickey, 1998; Hickey, 2000; Moody, 2020). The MDS method retains local variability and small-scale features as it does not use an average for calculating the slope. This method uses a 3x3 window but considers the center cell's elevation and its difference between one of the eight neighbors that give the maximum downhill slope. The consideration of only downhill neighbors for maximum value ensures that slope calculations are not overestimated (Dunn and Hickey, 1998; Hickey, 2000; Moody, 2020).

The slope value was calculated using Equation (4).

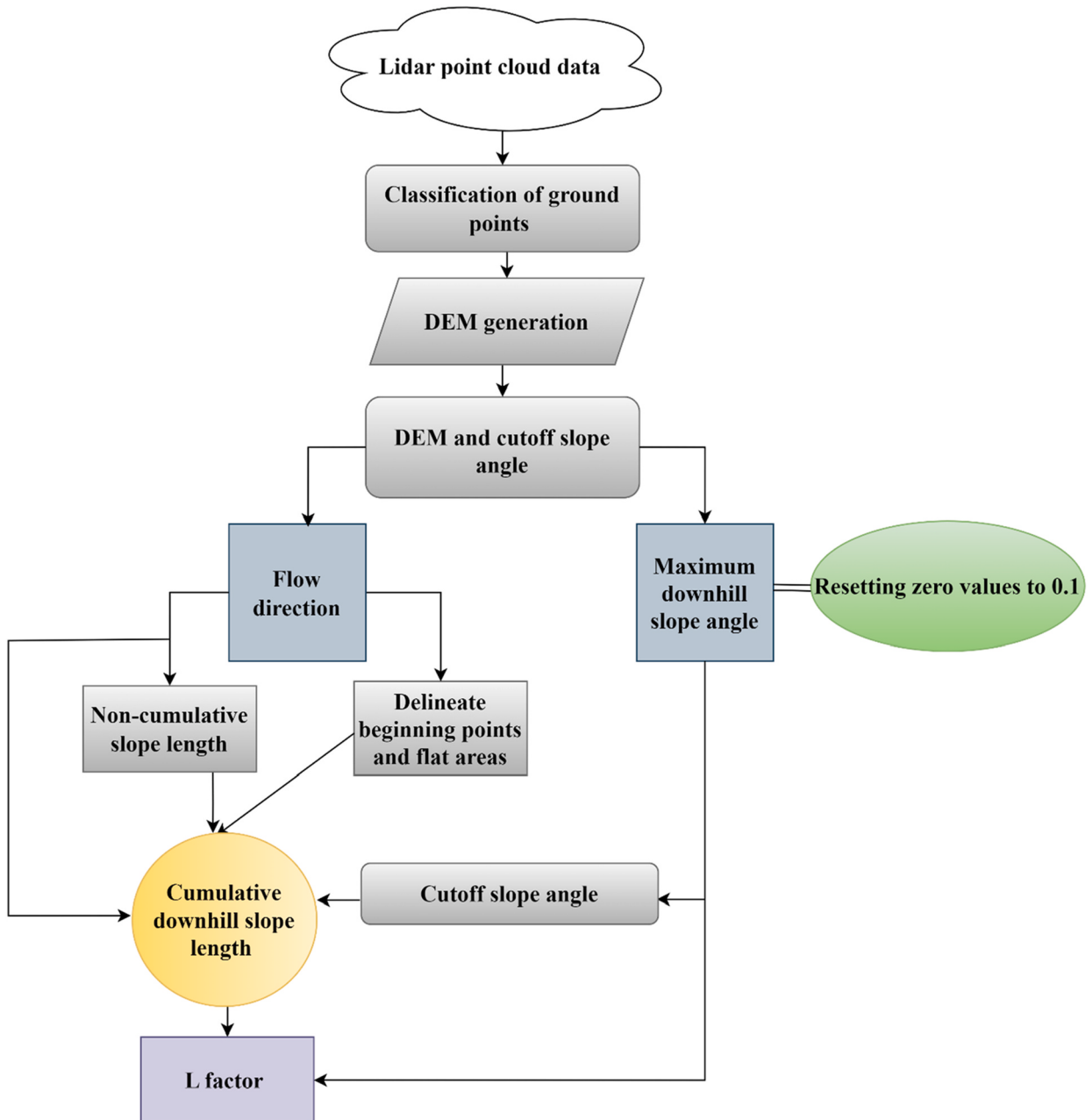


Fig. 3. Flowchart showing the process of L factor calculation.

$$\theta = \tan^{-1} \left(\frac{(Z_9 - Z_i)}{L_e} \right) \quad \text{Equation (4)}$$

Where, Z_9 represents elevation of the center cell and Z_i represents elevation of the neighboring cells (1 through 8). The distance to a neighboring cell (L_e) is determined by its position relative to the center cell, with diagonal distances adjusted by a factor of square root 2.

Once the slope value was obtained, the slope-steepness factor (S) was computed using the methodology described by [Kim and Maidment \(2014\)](#). Depending upon the slope condition, Equations (5) and (6) were applied:

$$S = 10.8 \sin \theta + 0.03 \text{ for slopes } \leq 9\% (5.15^\circ) \quad \text{Equation (5)}$$

$$S = 16.8 \sin \theta - 0.50 \text{ for slopes } > 9\% \quad \text{Equation (6)}$$

2.2.4. C and P factors

A CP factor raster layer for each harvest site was created by integrating field survey data with UAV data using GIS and deep learning techniques ([Fig. 4](#)).

The average C and P values for each harvest category were obtained through field surveys conducted following the USLE handbook ([Dissmeyer and Foster, 1984](#)). The harvest sites were divided into two categories, tilled (with topsoil removed) and untilled (without topsoil removal). Clear-cut (CC), CC with vegetation, and SMZs were categorized as untilled, while the other categories (roads, skid trails, and loading decks) were classified as tilled. Once the CP values for each harvest category were obtained, they were integrated into ArcGIS Pro 3.2 for further analysis.

For the analysis, all raster layers were clipped to the boundaries of the respective sites using the 'Extract by Mask' tool in ArcGIS Pro 3.2, utilizing the site boundary shapefiles. These layers were then resampled to a 0.5 m resolution and reprojected to the World Geodetic System (WGS) 1984 coordinate system, specifically Universal Transverse Mercator (UTM) Zone 16 N and UTM Zone 17 N, to ensure proper alignment of all data layers.

2.3. Model training and application

Six models based on U-Net, Deeplab V3, and PSPNet architectures, using ResNet-34 and ResNet-50 backbones were trained and evaluated for their segmentation accuracies. Once the best-performing model was identified, the orthomosaic map of each harvest site was segmented into different harvest categories. CP values collected from the field for each harvest category in each site were then integrated into GIS software to create CP raster layers. ArcGIS Pro 3.2 software was utilized to label sample data, train, and implement a deep learning model for segmenting harvest categories within a harvest site. The workflow for this process is illustrated in [Figs. 4 and 5](#).

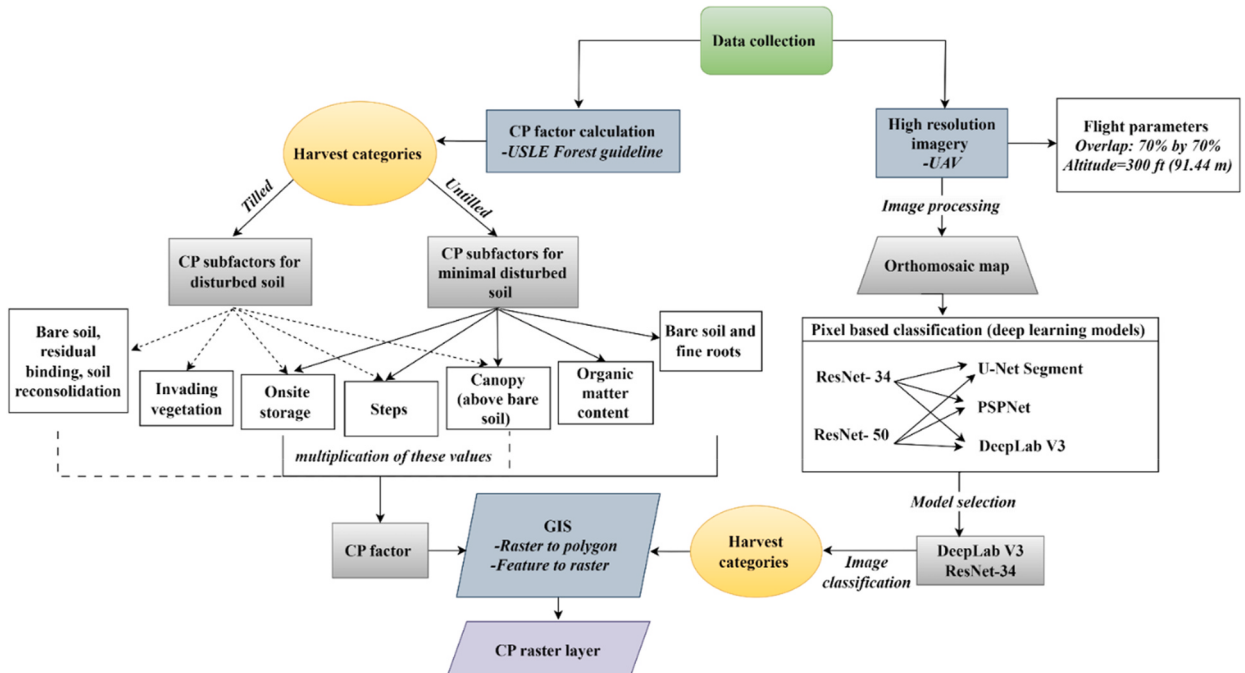


Fig. 4. Framework for harvest categories classification and CP raster layer preparation.

Initially, a clipping tool was used to extract sample images from each orthomosaic map to prepare the training and validation datasets. These sample images represented different harvest categories at each site. The images were labeled using the Image Collection Layer feature under the 'Label Objects for Deep Learning' tool. The training labels consisted of six harvest classes: SMZs, forest roads, CC, CC with vegetation, skid trails, and loading decks.

The labeled training samples were then transformed into training and validation datasets suitable for deep learning models using the 'Export Training Data for Deep Learning' tool in ArcGIS Pro 3.2. This process generated training datasets comprising a collection of labeled image chips that are compatible with model training tools in ArcGIS Pro 3.2. Default options were used for all training datasets:

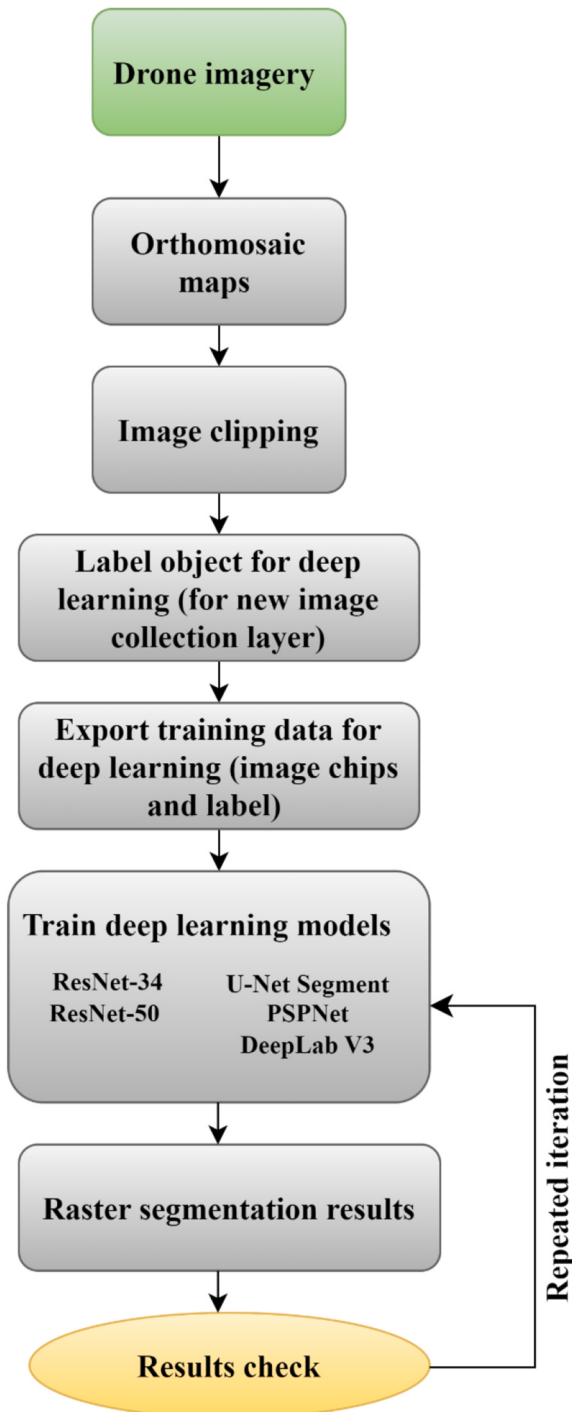


Fig. 5. Workflow for training deep learning models for harvest categories segmentation.

tile (image chip) size was set to 256×256 pixels, with a stride of 128 pixels in both the X and Y directions and the format was selected to be “classified tiles” (Figs. 6–8). To enhance the efficiency of the training process, transfer learning was used, allowing for the adjustment of pre-existing models to segment harvest categories with less training data than would be required to develop a model from scratch (Zhao et al., 2024). The ‘Train Deep Learning Model’ tool was used to train the models. The validation percentage was consistently set at 10% and the maximum number of epochs was fixed at 50. The learning rate field was left empty to allow the optimal learning rate to be determined automatically from the learning curve during training. The batch size was set to 8 throughout the training process.

2.4. Model accuracy and evaluation

To find the best model for segmenting harvest categories, we evaluated and compared 6 models using three metrics: precision, recall (sensitivity), and F1 score (Sun et al., 2023). Precision is a metric used to evaluate the accuracy of a classification model, specifically in identifying positive instances (Equation (7)). It measures the proportion of true positive predictions (correctly identified positive instances) out of all the instances that were predicted as positive by the model. Recall assesses the model’s ability to successfully detect pixels belonging to the target class and represents the recall rate for positive samples (Equation (8)). The F1 score is a metric used to evaluate the performance of a classification model by balancing both precision and recall (Equation (9)). These metrics were used to assess the performance of various models and identify the most suitable one for segmenting harvest categories. The model demonstrating the highest overall accuracy across all harvest categories was selected. This selected model was then used to segment each harvest site into its respective harvest categories.

$$\text{Precision} = \frac{\text{TP}}{\text{TP} + \text{FP}} \times 100\% \quad \text{Equation (7)}$$

$$\text{Recall} = \frac{\text{TP}}{\text{TP} + \text{FN}} \times 100\% \quad \text{Equation (8)}$$

$$\text{F1 score} = \frac{2 \times \text{TP}}{2 \times \text{TP} + \text{FP} + \text{FN}} \times 100\% \quad \text{Equation (9)}$$

Where, TP (True Positive) represents the number of pixels correctly classified as belonging to the intended class. FP (False Positive) refers to the number of pixels incorrectly classified as belonging to the intended class when they actually do not. FN (False Negative) denotes the number of pixels that belong to the intended class but were not correctly classified.

2.5. Erosion estimation

We used the raster calculator tool in ArcGIS Pro 3.2 to calculate potential soil erosion within each $0.5 \text{ m} \times 0.5 \text{ m}$ cell by multiplying the R, K, L, S, and CP raster layers, as described in Equation (1).

2.6. Hypothesis setup and statistical analysis

A hypothesis was formulated to test if there was a significant difference in erosion rates between different harvest categories, using a significance level of 0.05. Data were initially screened for outliers utilizing box plots and Z-scores. Subsequently, the Shapiro-Wilk test was conducted to evaluate normality using QQ plots and histograms (Shapiro and Wilk, 1965). For datasets meeting normality assumptions ($p > 0.05$), the Levene test was used to verify equal variances (Levene, 1960). When both normality and homogeneity of variance were confirmed ($p > 0.05$ in the Shapiro-Wilk and Levene tests), a two-sample *t*-test was considered (Walpole et al., 2012). If

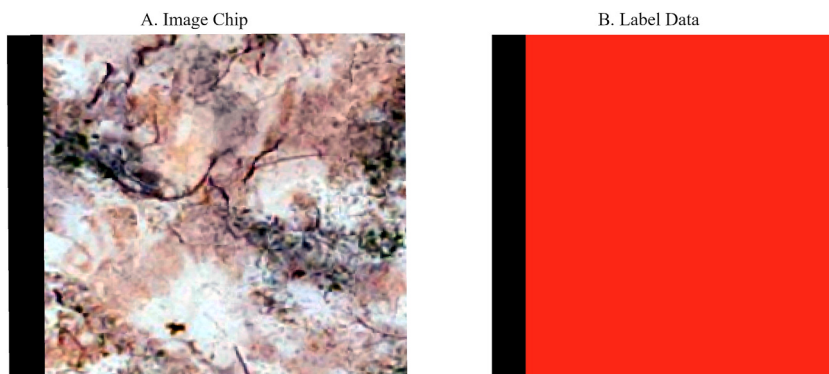


Fig. 6. Illustration of image chip of forest road and corresponding label data for training a deep learning model.

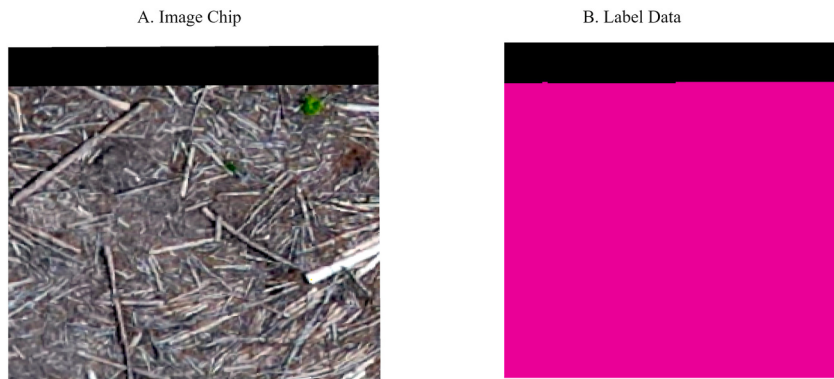


Fig. 7. Illustration of image chip of loading deck and corresponding label data for training a deep learning model.

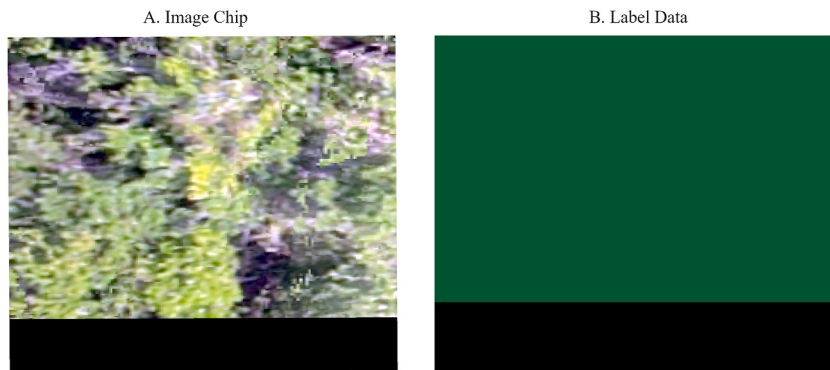


Fig. 8. Illustration of image chip of SMZs and corresponding label data for training a deep learning model.

the data did not meet normality assumptions ($p \leq 0.05$ in the Shapiro-Wilk test), Wilcoxon rank-sum test was used as a non-parametric alternative. Additionally, Kruskal-Wallis test was applied to detect significant differences among three or more independent groups (McKight and Najab, 2010). Following this, Dunn test with Bonferroni correction was performed for post-hoc analysis to identify specific differences (Dinno, 2015).



Fig. 9. Orthomosaic image of a harvest site.

3. Results

Although we conducted the study across all 20 sites, including maps and images of all sites would make the document excessively long. Therefore, we present the maps and images from one harvest site as a representative example (Figs. 9–12). The final soil erosion map of all harvest sites can be found in the supplementary materials.

3.1. Model comparison and selection

DeepLab V3 with a ResNet-34 backbone was selected based on its superior performance in precision, recall, and F1-score (Tables 1 and 2).

3.2. Harvest site example

3.2.1. R, K, LS, and CP factors and soil erosion rate

For the example harvest site, the average annual rainfall was recorded at 1524 mm, resulting in a calculated rainfall erosivity factor (R) of 8264.22 MJ mm/ha·hr·yr.

The soil erodibility factor (K) map illustrates the spatial distribution of the K factor across the harvest site (Fig. 10). The K factor values, represented in different colors, indicate varying levels of soil susceptibility to erosion. Areas with higher values are more prone to erosion.

Fig. 11 (a) and (b) present the spatial distribution maps of the slope-length factor (L) and the slope-steepness factor (S) across the harvest site. The L factor values are color-coded, with higher values shown in shades of red and yellow and lower values in shades of green and blue (Fig. 11 a). Areas with higher L values correspond to longer slope lengths, which contribute to a greater potential for soil erosion.

Similar to the L factor map, the S factor values are color-coded, with higher values represented by red and yellow, and lower values by green and blue (Fig. 11 b). The S factor values indicate the steepness of the slopes, with steeper areas displaying higher values. These areas are more prone to soil erosion due to the increased gravitational force acting on soil particles.

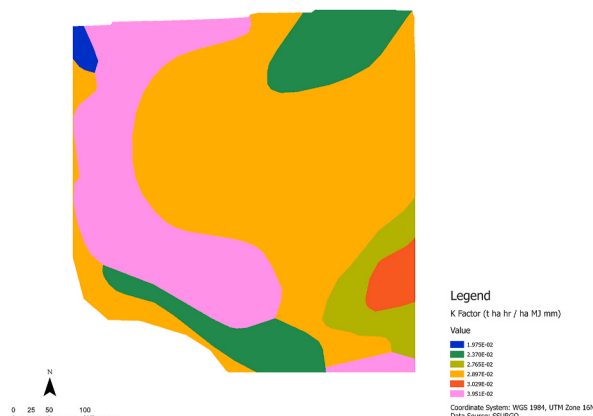
The map showing the CP factor illustrates the spatial distribution of CP values across the harvest site (Fig. 12 a). Evaluating the specific harvest site, the highest CP factor was observed in the forest roads, with an average value of 0.433. In contrast, SMZ exhibited the lowest CP factor, with an average value of 0.00003. Additionally, soil erosion rates (t/ha/yr) across different harvest categories within the example harvest site highlighted variations in soil erosion rates among the categories (Fig. 12 a). SMZ had the lowest erosion rate at 0.018 t/ha/yr, while roads had the highest erosion rate among all categories, at 23.70 t/ha/yr.

Soil erosion rate maps illustrate the spatial distribution of soil erosion rates (t/ha/yr) across the harvest site (Fig. 12 b). Green areas indicate lower erosion rates and red areas indicate higher erosion rates. The average soil erosion rate across the harvest site example was 1.59 t/ha/yr.

3.3. Average CP factor and soil erosion rates across harvest sites: documentation and comparisons

The analysis of average CP factor values across 20 harvest sites revealed that forest roads had the highest average CP factor at 0.268. In contrast, both the CC area with vegetation and SMZ exhibited the lowest average CP factor values, each at 0.001, reflecting minimal erosion susceptibility (Table 3).

Soil erosion rates (t/ha/yr) were calculated across different harvest categories for all 20 harvest sites (Table 4). Roads exhibited the highest mean erosion rate at 13.17 t/ha/yr. Skid trails followed with a mean erosion rate of 4.12 t/ha/yr and loading decks had a mean erosion rate of 1.07 t/ha/yr. CC and CC with vegetation showed lower mean erosion rates of 0.19 t/ha/yr and 0.11 t/ha/yr,



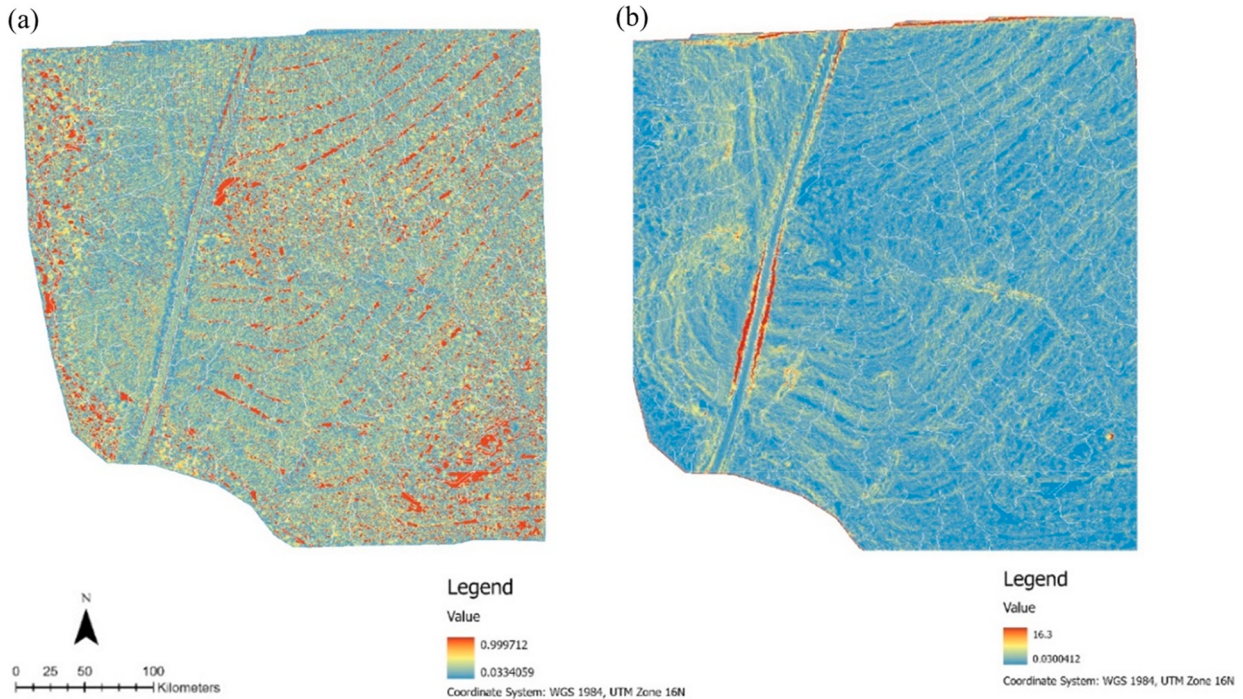


Fig. 11. (a): Map showing slope-length factor (L) of the harvest site, (b): Map showing slope-steepness factor (S) of the harvest site.

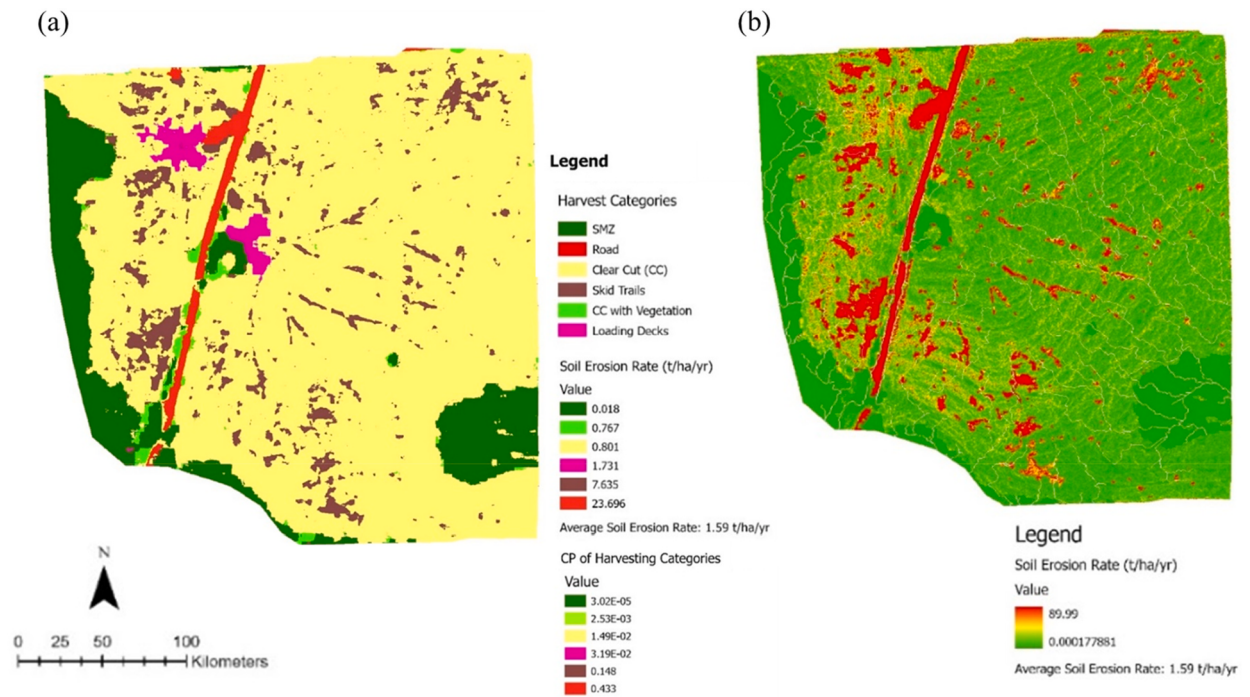


Fig. 12. (a): Map showing the CP factor and soil erosion rate (t/ha/yr) of the harvest site according to harvest categories, (b): Map showing soil erosion rate (t/ha/yr) of the harvest site.

respectively. SMZs showed the lowest mean erosion rate at 0.02 t/ha/yr.

Comparing soil erosion rates across different harvest categories revealed significant differences in the rankings of erosion rates among these categories. Specifically, the categories 'road', 'skid trail', and 'loading deck' exhibited significantly higher erosion rates

Table 1

Performance metrics of pixel-based classification models for different harvest categories.

Harvest categories	Pixel based classification model	Backbone network	Precision	Recall	F1
SMZ	U-Net	ResNet-34	0.991	0.987	0.989
SMZ	U-Net	ResNet-50	0.970	0.955	0.962
SMZ	DeepLab V3	ResNet-34	0.976	0.982	0.979
SMZ	DeepLab V3	ResNet-50	0.971	0.981	0.976
SMZ	PSPNet	ResNet-34	0.871	0.965	0.916
SMZ	PSPNet	ResNet-50	0.989	0.831	0.903
Road	U-Net	ResNet-34	0.931	0.957	0.944
Road	U-Net	ResNet-50	0.984	0.896	0.938
Road	DeepLab V3	ResNet-34	0.987	0.983	0.985
Road	DeepLab V3	ResNet-50	0.931	0.957	0.944
Road	PSPNet	ResNet-34	0.952	0.936	0.944
Road	PSPNet	ResNet-50	0.802	0.988	0.885
Clear Cut (CC)	U-Net	ResNet-34	0.975	0.986	0.981
Clear Cut (CC)	U-Net	ResNet-50	0.922	0.973	0.947
Clear Cut (CC)	DeepLab V3	ResNet-34	0.978	0.989	0.983
Clear Cut (CC)	DeepLab V3	ResNet-50	0.981	0.986	0.983
Clear Cut (CC)	PSPNet	ResNet-34	0.922	0.958	0.939
Clear Cut (CC)	PSPNet	ResNet-50	0.936	0.838	0.884
CC with Vegetation	U-Net	ResNet-34	0.973	0.977	0.975
CC with Vegetation	U-Net	ResNet-50	0.879	0.933	0.905
CC with Vegetation	DeepLab V3	ResNet-34	0.982	0.954	0.968
CC with Vegetation	DeepLab V3	ResNet-50	0.972	0.960	0.966
CC with Vegetation	PSPNet	ResNet-34	0.923	0.840	0.879
CC with Vegetation	PSPNet	ResNet-50	0.88	0.862	0.871
Skid Trail	U-Net	ResNet-34	0.883	0.772	0.824
Skid Trail	U-Net	ResNet-50	0.591	0.377	0.460
Skid Trail	DeepLab V3	ResNet-34	0.954	0.855	0.902
Skid Trail	DeepLab V3	ResNet-50	0.893	0.888	0.891
Skid Trail	PSPNet	ResNet-34	0.621	0.336	0.436
Skid Trail	PSPNet	ResNet-50	0.644	0.374	0.446
Loading Deck	U-Net	ResNet-34	0.881	0.941	0.910
Loading Deck	U-Net	ResNet-50	0.994	0.995	0.995
Loading Deck	DeepLab V3	ResNet-34	0.966	0.979	0.973
Loading Deck	DeepLab V3	ResNet-50	0.717	0.833	0.771
Loading Deck	PSPNet	ResNet-34	0.985	0.989	0.987
Loading Deck	PSPNet	ResNet-50	0.943	0.944	0.933

Table 2

The best performance metrics for the selected model across different harvest categories.

Harvest categories	Precision	Recall	F1
Clear Cut (CC)	0.978	0.989	0.983
CC with Vegetation	0.982	0.954	0.968
Road	0.987	0.983	0.985
Skid Trail	0.954	0.855	0.902
Loading Deck	0.966	0.979	0.973
SMZ	0.976	0.982	0.979

Table 3

Average CP factor values across different harvest categories from all harvest sites (N = 20).

Harvest categories	CP factors average values
Clear Cut (CC)	0.004
CC with Vegetation	0.001
Road	0.268
Skid Trail	0.146
Loading Deck	0.024
SMZ	0.001

compared to other categories ($p \leq 0.05$) (Table 5).

The overall average erosion rate from all the harvest sites (N = 20) was 0.78 t/ha/yr (min = 0.04 t/ha/yr, max = 2.17 t/ha/yr, Table 6).

Table 4

Statistical parameters of soil erosion rates (t/ha/yr) across different harvest categories (N = 20).

Harvest categories	Statistical parameters				
	Mean erosion (t/ha/yr)	Standard error of mean	Minimum (t/ha/yr)	Median (t/ha/yr)	Maximum (t/ha/yr)
Clear Cut (CC)	0.19	0.04	0.02	0.11	0.77
CC with Vegetation	0.11	0.04	0.00	0.05	0.80
Road	13.17	2.04	1.38	12.07	36.03
Skid Trail	4.12	0.59	0.45	3.25	10.34
Loading Deck	1.07	0.19	0.03	1.14	3.38
SMZ	0.02	0.01	0.00	0.01	0.17

4. Discussion

4.1. New approach for forest soil erosion estimation

Traditionally, soil erosion estimation has depended on field-based surveys, which, although very common, are field-intensive and time-consuming. Conventional field-based erosion estimation methods often rely on sample plots, where increasing the number of plots improves accuracy but can be field-intensive and time consuming, while fewer plots can lead to less accurate estimates. Additionally, human factors can impact field coverage and data accuracy. This may lead to an incomplete understanding of the ongoing erosion processes. This study demonstrated the use of deep learning techniques to segment harvest sites into various categories with high-resolution UAV imagery and to estimate potential soil erosion from each category using GIS software.

Recently, deep learning techniques have been extensively used in image segmentation. CNNs, in particular, have shown exceptional performance in remote sensing image classification tasks due to their hierarchical feature extraction capability, parameter sharing, and local connectivity mechanisms within convolutional layers (Boulila et al., 2021; O'shea & Nash, 2015). Previous studies combining GIS and remote sensing to estimate soil erosion have primarily focused on broad LULC classifications, often treating forested areas as a single entity. However, within timber harvest tracts, there are distinct categories, such as forest roads, skid trails, loading decks, SMZs, and CC areas. These categories have varying potentials for soil erosion, as demonstrated by field-based erosion studies (Fielding et al., 2022; Parajuli et al., 2024). High-resolution imagery is useful for differentiating these harvest categories, as aerial imagery with high spatial resolution allows for better observation of a harvest site, capturing fine details (Samarin et al., 2020). Such imagery can be collected from various platforms, including satellites and UAVs (Guirado et al., 2017; Rijal et al., 2023). While satellite imagery is useful, it comes with challenges, such as data unavailability for specific dates, the requirement for large coverage in tasking orders, and the limited resolution of freely accessible satellite data. In contrast, UAV-based imagery offers greater flexibility and higher precision in distinguishing different harvest categories. These days, UAVs are available in a variety of sizes, becoming more affordable, and increasingly efficient at collecting high-resolution imagery at specific time period (Rijal et al., 2023).

In our study, high-resolution imagery captured by a UAV enabled detailed analysis, allowing for the precise delineation of areas with high erosion potential. In soil erosion assessment, remote sensing-based semantic segmentation tasks are highly effective for mapping erosion across diverse terrains. Our findings showed that the DeepLab V3 model with a ResNet-34 backbone performed best to segment a harvest site into various harvesting categories, achieving an F1 score of over 90% in all harvest categories. This approach offers enhanced maneuverability and flexibility, improving the ability to monitor and map erosion-prone areas while providing crucial data for informed decision-making and sustainable land management practices.

4.2. Analysis of soil erosion rates across different harvest categories

This study revealed significant differences in soil erosion rates across various harvest categories. Our findings are consistent with different field-based studies, which have also identified the highest erosion rates on forest roads, skid trails, and loading decks, and the lowest rates in SMZs (Fielding et al., 2022; Garren et al., 2022; Parajuli et al., 2024). Roads, skid trails, and loading decks exhibited significantly higher erosion rates, as indicated by positive mean rank differences and significant p-values, compared to categories like CC areas with vegetation and CC areas without vegetation. The highest erosion rate from these categories can be attributed to intense topsoil disturbance, primarily due to the frequent passes of heavy machinery (Parajuli et al., 2022; Sakai et al., 2008). In contrast, SMZs consistently demonstrated the lowest erosion rates, characterized by negative mean rank differences and significant p-values relative to other harvest categories (Table 5). This lower erosion rate in SMZs is likely due to minimal soil disturbance and the protective vegetative cover typical of SMZs, which helps to stabilize the soil and prevent erosion.

The lack of statistical significance between certain category pairs, such as CC areas with and without vegetation and skid trails compared to roads, suggests similar post-harvest characteristics and erosion rates between these categories. This similarity may result from comparable levels of soil disturbance and ground cover conditions. These findings highlight the importance of evaluating both the intensity and nature of harvesting activities when assessing their impact on soil erosion.

4.3. Discrepancies between field-based and GIS-based erosion rates

This study, using a GIS-based method for erosion estimation, resulted an average erosion rate of 0.78 t/ha/year (min = 0.04, max =

Table 5

Erosion rate differences across harvest categories were determined using pairwise multiple comparison post-hoc analysis with Dunn's test, following the Kruskal-Wallis test at a significance level of $\alpha = 0.05$. An asterisk (*) indicates significant p-values.

Harvest categories	Mean rank differences	p-values
Clear Cut-CC with Vegetation	1.04	1.0000
Loading Deck-CC with Vegetation	3.05	0.0169*
Loading Deck-Clear Cut	2.01	0.3327
Road-CC with Vegetation	6.74	0.0000*
Road-Clear Cut	5.70	0.0000*
Road-Loading Deck	3.69	0.0017*
Skid Trail-CC with Vegetation	5.32	0.0000*
Skid Trail-Clear Cut	4.28	0.0001*
Skid Trail-Loading Deck	2.27	0.1755
Skid Trail-Road	-1.42	1.0000
SMZ-CC with Vegetation	-1.54	0.9301
SMZ-Clear Cut	-2.50	0.0921
SMZ-Loading Deck	-4.37	0.0001*
SMZ-Road	-7.78	0.0000*
SMZ-Skid Trail	-6.46	0.0000*

Table 6

Comparison of GIS-based and field-based soil erosion rates (tonnes/ha/year) across harvest sites (N = 20).

Sites	GIS-based average erosion rate (tonnes/ha/year)	Field-based average erosion rate (tonnes/ha/year)
1	0.24	0.19
2	0.41	0.20
3	0.28	0.13
4	0.04	0.09
5	0.10	0.04
6	0.63	0.44
7	0.40	0.14
8	0.70	0.20
9	0.97	0.06
10	1.36	0.24
11	0.96	0.57
12	1.59	0.69
13	0.45	0.23
14	1.02	0.84
15	0.58	0.41
17	0.53	0.26
18	2.17	0.26
18	1.78	0.71
19	1.06	0.66
20	0.42	0.33
Average	0.78	0.33

2.17) across the harvest sites. In comparison, the field-based method resulted a lower average erosion rate of 0.33 t/ha/year (min = 0.04, max = 0.84, Table 6).

These differences between the erosion rates obtained from GIS-based and field-based methods can be attributed to variations in data sources, spatial resolution, and methodologies used for data collection. The higher spatial resolution and localized detail of GIS-based methods enable the capture of local variations in rainfall, soil properties, and topography, providing a more detailed information. The field-based method relies on R-factor values from USLE guidelines, determined by manually tracking the harvest site locations. Relying solely on the average annual rainfall index values from the USLE handbook may not reflect current conditions, as rainfall patterns can change over time (EPA, 2023). To obtain more reliable soil erosion estimates, it is essential to incorporate the latest rainfall data, ensuring a more accurate representation of recent trends and conditions.

In the field-based method, identifying different soil types and soil erodibility factor (K) values within a harvest site was challenging. As a result, a single K value was applied across the entire harvest site, assuming homogeneous soil characteristics. In contrast, the GIS-based method utilized detailed soil information from the SSURGO, accounting for the spatial variability of K values within a harvest site. Similarly, field-based methods commonly rely on manual tools, such as clinometers and measuring tapes, to calculate slope length and steepness, which are susceptible to human error. On the other hand, the GIS-based method incorporated LiDAR to generate DEM of the harvest site, enabling the use of advanced techniques like grid accumulation and maximum downhill slope methods for more accurate and detailed topographic analysis.

The field-based method remains a crucial approach for studying soil erosion, offering valuable on-site observations and ground-truthing. However, its reliability can be affected if an insufficient number of samples are collected, particularly in capturing site-

wide variations. GIS and remote sensing are used to capture the entire site's topography, enabling a full-scale analysis rather than relying on small sample areas. This may also explain why the GIS-based method resulted different erosion rate as compared to field-based method. In addition to providing more accurate estimates, the GIS-based method also offers the advantage of creating detailed erosion maps for future reference. These maps can be used to develop long-term management strategies, allowing for the comparison of erosion rates across multiple harvest seasons. By providing a permanent record of soil erosion from a harvest site, GIS-based methods contribute to more effective decision-making and resource management over time. Overall, the methodology developed in this study highlights the advantages of using a holistic, technology-driven approach to improve the accuracy of erosion assessments.

4.4. CP factor documentation

When adapting the USLE model to local conditions, it is critical to gather accurate data on rainfall, soil erodibility, slope factors, and management practices. While information on rainfall, soil, and slope is widely accessible online, acquiring reliable CP factor data requires careful consideration due to its dependency on specific site characteristics, the extent and degree of disturbance within a harvest site, and other management conditions. CP factors, for instance, are influenced by numerous sub-factors, including previous management practices, bare soil, onsite storage, organic matter, steps, vegetative canopy, surface cover, surface roughness, and soil moisture (Dissmeyer and Foster, 1984). No online database currently provides CP factor information based on specific site or soil conditions, necessitating field surveys for data collection.

Several past studies have generalized C and P values for entire forest areas. Ganasri and Ramesh (2016) assigned a C value of 0.003 and a P value of 1 for the entire forest area in western India. Similarly, Kim and Maidment (2014) applied these values uniformly across deciduous, evergreen, and mixed forests in central Texas. These approaches can provide a broad understanding of soil erosion potential but may not fully provide the detailed information required to identify areas within a harvest site that are more susceptible to erosion. This study calculated and documented the CP values for each harvest category within a harvest site. Results from the study indicated that CP values varied across different harvest site categories. Forest roads exhibited the highest CP value at 0.268, indicating their high contribution to soil erosion potential due to the absence of canopy cover and the physical disturbances caused by road construction and use. In contrast, SMZs and CC with vegetation recorded the lowest CP values at 0.001, reflecting their minimal contribution to soil erosion risk by offering protective vegetation cover and enhanced stability. This highlights the effectiveness of vegetation and canopy cover in these areas as crucial measures for erosion control and highlights their role in mitigating soil erosion risks.

This study emphasizes the need to assign specific CP values for different harvest categories taking into account their unique characteristics and conditions. This adaptation is crucial as it addresses the heterogeneity within forest landscapes and reflects the actual management and soil disturbance levels. The CP values obtained in this research can be used in estimating soil erosion from a harvest site using remote sensing techniques in similar areas. Although this study was primarily focused on harvest sites located in the Coastal Plain region of the southeastern US, expanding this research to include different physiographic regions and states will greatly enhance the overall understanding and practical application of CP values. This documentation provides forest managers and researchers with a more efficient method for estimating soil erosion at forest harvest sites. It facilitates the implementation of soil conservation strategies and best management practices according to specific site conditions and soil characteristics.

4.5. Challenges and future directions

In field-based forest soil erosion studies, stream crossings are often categorized separately. However, in our study, distinguishing stream crossings from SMZs was difficult because the imagery was captured from a top-down perspective, where overlapping canopy cover obscured the underlying features and their conditions, as also noted by Rijal et al. (2023). Hence, stream crossings were not classified as a separate category in this study. Differentiating features under dense canopy cover remains challenging and may demand imagery collected at different view settings. While this study provides an effective alternative approach to conventional soil erosion assessments, it faces challenges like the need for high-quality, high-resolution data, which poses logistical and financial constraints in large forest areas. Future research could explore using medium-resolution imagery combined with supplementary data sources, such as multispectral or hyperspectral data, to improve the segmentation and classification of harvest categories.

5. Conclusions

In this study, we integrated high-resolution imagery, deep learning, and GIS with the USLE model to analyze and visualize potential soil loss, demonstrating the practical application of these technologies in forest management. Utilizing the DeepLab V3 architecture with a ResNet-34 backbone, we achieved high performance in detecting and differentiating forest harvest site categories. Furthermore, our findings revealed significant variability in erosion rates, with forest roads and skid trails showing higher susceptibility to erosion.

This study documented average CP values for each harvest category to support GIS-based soil erosion estimation in the Coastal Plain region. Although this approach minimizes the need for extensive field collection of CP values, site-specific field data remain indispensable. Field measurements are critical for validating and calibrating GIS-based methods, ensuring their accuracy and reliability.

The techniques developed in this study to generate spatially detailed erosion risk maps can greatly improve decision-making for forest managers. By identifying high-risk areas, managers can prioritize erosion control measures, such as strategically planning harvesting techniques to minimize soil disturbance. Additionally, continuous monitoring of forest soil conditions using UAVs provides a valuable tool for assessing the effectiveness of management practices over time. UAV-derived orthomosaic images and DEMs can

support forest managers in planning skid trails, road networks, loading deck installations, and identifying erosion-prone areas.

This study thus enhances the accuracy and applicability of the USLE model by integrating advanced remote sensing technologies, GIS, and deep learning models. While these modern tools provide significant benefits for forestry decision-making, they should complement, not replace, field-collected data. Together, these methods offer forest managers robust decision-support tools to address environmental challenges while ensuring sustainable forest operations.

CRediT authorship contribution statement

Manisha Parajuli: Writing – review & editing, Writing – original draft, Visualization, Validation, Resources, Methodology, Investigation, Formal analysis, Data curation, Conceptualization. **Richard Cristan:** Writing – review & editing, Validation, Supervision, Software, Resources, Methodology, Investigation, Conceptualization. **Marissa Jo Daniel:** Writing – review & editing, Validation, Supervision. **Arjun Rijal:** Writing – review & editing, Visualization, Validation, Methodology, Formal analysis, Data curation, Conceptualization, Investigation. **Dana Mitchell:** Writing – review & editing, Validation, Supervision. **Timothy McDonald:** Writing – review & editing, Supervision. **Tom Gallagher:** Writing – review & editing, Validation, Supervision, Software, Resources, Project administration, Methodology, Investigation, Funding acquisition, Conceptualization.

Declaration of competing interest

All the authors declare that they have no known competing financial interests or personal relationships that could have appeared to influence the work reported in this paper.

Acknowledgment

This research work was funded by the USDA National Institute of Food and Agriculture [2019-67020-29287].

Data availability

Data will be made available on request.

References

- Althoff, D., Rodrigues, L.N., da Silva, D.D., 2021. Addressing hydrological modeling in watersheds under land cover change with deep learning. *Adv. Water Resour.* 154, 103965.
- Barrett, S.M., Aust, W.M., Bolding, M.C., Lakel III, W.A., Munsell, J.F., 2016. Estimated erosion, ground cover, and best management practices audit details for postharvest evaluations of biomass and conventional clearcut harvests. *J. For.* 114 (1), 9–16.
- Binkley, D., Brown, T.C., 1993. Forest practices as nonpoint sources of pollution in North America 1. *JAWRA J. Am. Water Res. Assoc.* 29 (5), 729–740.
- Blaszcynski, J., 2001. Regional Sheet and Rill Soil Erosion Prediction with the Revised Universal Soil Loss Equation (RUSLE)-GIS Interface. US Department of the Interior. Bureau of Land Management, National Science.
- Bouguettaya, A., Zarzour, H., Kechida, A., Taberkit, A.M., 2022. Deep learning techniques to classify agricultural crops through UAV imagery: a review. *Neural Comput. Appl.* 34 (12), 9511–9536. <https://doi.org/10.1007/s00521-022-07104-9>.
- Boullila, W., Sellami, M., Driss, M., Al-Sarem, M., Safaei, M., Ghaleb, F.A., 2021. RS-DCNN: a novel distributed convolutional-neural-networks based-approach for big remote-sensing image classification. *Comput. Electron. Agric.* 182, 106014.
- Cooper, K., 2011. Evaluation of the Relationship between the RUSLE R-Factor and Mean Annual Precipitation. Colorado State University, Fort Collins.
- Cristan, R., Aust, W.M., Bolding, M.C., Barrett, S.M., Munsell, J.F., Schilling, E., 2016. Effectiveness of forestry best management practices in the United States: literature review. *For. Ecol. Manag.* 360, 133–151.
- Dinno, A., 2015. Nonparametric pairwise multiple comparisons in independent groups using Dunn's test. *STATA J.* 15 (1), 292–300.
- Dissmeyer, G.E., Foster, G.R., 1984. A Guide for Predicting Sheet and Rill Erosion on Forest Land. A. USDA Forest Service Forestry Technical Publication, p. 40. R8-TP 6, Georgia.
- Duarte, L., Cunha, M., Teodoro, A.C., 2021. Comparing hydric erosion soil loss models in rainy mountainous and dry flat regions in Portugal. *Land* 10 (6), 554.
- Dunn, M., Hickey, R., 1998. The effect of slope algorithms on slope estimates within a GIS. *Cartography* 27 (1), 9–15. <https://doi.org/10.1080/00690805.1998.9714086>.
- EPA, 2023. Climate Change Indicators. U.S. and Global Precipitation. Retrieved 06/18 from. <https://www.epa.gov/climate-indicators/climate-change-indicators-us-and-global-precipitation>.
- Esri, 2022. ArcGIS Drone2Map, 2022, Version 2022.1.2. <https://www.esri.com/en-us/arcgis/products/arcgis-drone2map>.
- Farhan, Y., Nawaiseh, S., 2015. Spatial assessment of soil erosion risk using RUSLE and GIS techniques. *Environ. Earth Sci.* 74, 4649–4669.
- Fielding, J.A., Hawks, B.S., Aust, W.M., Bolding, M.C., Barrett, S.M., 2022. Estimated erosion from clearcut timber harvests in the southeastern United States. *For. Sci.* 68 (3), 334–342.
- Ganasri, B.P., Ramesh, H., 2016. Assessment of soil erosion by RUSLE model using remote sensing and GIS - a case study of Nethravathi Basin. *Geosci. Front.* 7 (6), 953–961. <https://doi.org/10.1016/j.gsf.2015.10.007>.
- Garren, A.M., Bolding, M.C., Barrett, S.M., Aust, W.M., Coates, T.A., 2022. Best management practices, estimated erosion, residual woody debris, and ground cover characteristics following biomass and conventional clearcut harvests in Virginia's mountains. *For. Sci.* 68 (3), 299–311.
- Guirado, E., Tabik, S., Alcaraz-Segura, D., Cabello, J., Herrera, F., 2017. Deep-learning versus OBIA for scattered shrub detection with google earth imagery: ziziphus lotus as case study. *Remote Sens.* 9 (12), 1220. <https://www.mdpi.com/2072-4292/9/12/1220>.
- Guo, Q., Zhang, J., Guo, S., Ye, Z., Deng, H., Hou, X., Zhang, H., 2022. Urban tree classification based on object-oriented approach and random forest algorithm using unmanned aerial vehicle (uav) multispectral imagery. *Remote Sens.* 14 (16), 3885.
- Hawks, B.S., Aust, W.M., Bolding, M.C., Barrett, S.M., Schilling, E., Fielding, J.A.H., 2022. Linkages between forestry best management practices and erosion in the southeastern U.S. *J. Environ. Manag.* 305, 114411. <https://doi.org/10.1016/j.jenvman.2021.114411>.
- Hickey, R., 2000. Slope angle and slope length solutions for GIS. *Cartography* 29 (1), 1–8. <https://doi.org/10.1080/00690805.2000.9714334>.
- Hiesl, P., Benjamin, J.G., 2013. Applicability of international harvesting equipment productivity studies in Maine, USA: a literature review. *Forests* 4 (4), 898–921.

- Jeppesen, J.H., Jacobsen, R.H., Inceoglu, F., Toftegaard, T.S., 2019. A cloud detection algorithm for satellite imagery based on deep learning. *Remote Sens. Environ.* 229, 247–259.
- Khosravi, K., Rezaie, F., Cooper, J.R., Kalantari, Z., Abolfathi, S., Hatamiafkouieh, J., 2023. Soil water erosion susceptibility assessment using deep learning algorithms. *J. Hydrol.* 618, 129229.
- Kim, Y., Maidment, D., 2014. Soil erosion assessment using GIS and revised universal soil loss equation (RUSLE). *CE 394K GIS in Water Resources*, David R. Maidment 5.
- Lafren, J.M., Elliot, W., Flanagan, D., Meyer, C., Nearing, M., 1997. WEPP-predicting water erosion using a process-based model. *J. Soil Water Conserv.* 52 (2), 96–102.
- Levene, H., 1960. Robust tests for equality of variances. *Contribut. Probab. Statist.* 278–292.
- Li, J., Xiong, M., Sun, R., Chen, L., 2024. Temporal variability of global potential water erosion based on an improved USLE model. *Int. Soil Water Conserva. Res.* 12 (1), 1–12.
- Ma, L., Liu, Y., Zhang, X., Ye, Y., Yin, G., Johnson, B.A., 2019. Deep learning in remote sensing applications: a meta-analysis and review. *ISPRS J. Photogrammetry Remote Sens.* 152, 166–177. <https://doi.org/10.1016/j.isprsjprs.2019.04.015>.
- Ma, Z., Mei, G., 2021. Deep learning for geological hazards analysis: data, models, applications, and opportunities. *Earth Sci. Rev.* 223, 103858.
- Malinowski, R., Heckrath, G., Rybicki, M., Eltner, A., 2023. Mapping rill soil erosion in agricultural fields with UAV-borne remote sensing data. *Earth Surf. Process. Landf.* 48 (3), 596–612. <https://doi.org/10.1002/esp.5505>.
- McCool, D., Foster, G., Yoder, D., Weesies, G., McGregor, K., Bingner, R., 2004. The Revised Universal Soil Loss Equation, Version 2. In: *Proceedings of the 13th International Soil Conservation Organization Conference*, July 4–8, 2004. Paper No. 665, Brisbane, Australia.
- McKnight, P.E., Najab, J., 2010. Kruskal-wallis Test. *The Corsini Encyclopedia of Psychology*, 1–1.
- McWilliams, W.H., 1992. Forest Resources of Alabama, vol. 170. US Department of Agriculture, Forest Service. Southern Forest Experiment Station.
- Moody, A., 2020. Comparing Rusle LS Calculation Methods across Varying DEM Resolutions.
- Murray, J., Hiesl, P., Hagan, D., Baldwin, R., 2023. Assessing productivity and cost of timber harvesting during longleaf pine ecosystem restoration. *Int. J. For. Eng.* 34 (2), 117–129. <https://doi.org/10.1080/14942119.2022.2157184> [Article].
- O'shea, K., Nash, R., 2015. An Introduction to Convolutional Neural Networks. *arXiv preprint arXiv:1511.08458*.
- Panagos, P., Meusburger, K., Alewell, C., Montanarella, L., 2012. Soil erodibility estimation using LUCAS point survey data of Europe. *Environ. Model. Software* 30, 143–145.
- Parajuli, M., 2021. *Operational And Environmental Impacts Of Whole Tree Harvesting In the Southern United States* [Masters of Science in Forest Resources. Clemson University, USA. https://open.clemson.edu/cgi/viewcontent.cgi?article=4605&context=all_theses.
- Parajuli, M., Gallagher, T., Cristan, R., Daniel, M.J., Mitchell, D., McDonald, T., Rijal, A., Zheng, J., 2024. Postharvest evaluations of soil erosion, ground cover, and best management practice implementation on integrated biomass and conventional clearcut harvest sites. *For. Ecol. Manag.* 566, 122041.
- Parajuli, M., Hiesl, P., Hagan, D., Khanal, P., 2022. Logging Operations and Soil Compaction.
- Pearse, G.D., Tan, A.Y.S., Watt, M.S., Franz, M.O., Dash, J.P., 2020. Detecting and mapping tree seedlings in UAV imagery using convolutional neural networks and field-verified data. *ISPRS J. Photogrammetry Remote Sens.* 168, 156–169. <https://doi.org/10.1016/j.isprsjprs.2020.08.005>.
- Pinson, A.O., AuBuchon, J.S., 2023. A new method for calculating C factor when projecting future soil loss using the Revised Universal soil loss equation (RUSLE) in semi-arid environments. *Catena* 226, 107067. <https://doi.org/10.1016/j.catena.2023.107067>.
- Rawat, K.S., Mishra, A.K., Bhattacharyya, R., 2016. Soil erosion risk assessment and spatial mapping using LANDSAT-7 ETM+, RUSLE, and GIS—a case study. *Arabian J. Geosci.* 9, 1–22.
- Renard, K.G., 1997. Predicting Soil Erosion by Water: a Guide to Conservation Planning with the Revised Universal Soil Loss Equation (RUSLE). US Department of Agriculture, Agricultural Research Service.
- Renard, K.G., Freimund, J.R., 1994. Using monthly precipitation data to estimate the R-factor in the revised USLE. *J. Hydrol.* 157 (1), 287–306. [https://doi.org/10.1016/0022-1694\(94\)90110-4](https://doi.org/10.1016/0022-1694(94)90110-4).
- Rijal, A., Cristan, R., Gallagher, T., Narine, L.L., Parajuli, M., 2023. Evaluating the feasibility and potential of unmanned aerial vehicles to monitor implementation of forestry best management practices in the coastal plain of the southeastern United States. *For. Ecol. Manag.* 545, 121280.
- Sakai, H., Nordfjell, T., Suadicani, K., Talbot, B., Bøllehuus, E., 2008. Soil compaction on forest soils from different kinds of tires and tracks and possibility of accurate estimate. *Croat. J. For. Eng.: J. Theory Appl. Forestry Eng.* 29 (1), 15–27.
- Samarin, M., Zweifel, L., Roth, V., Alewell, C., 2020. Identifying soil erosion processes in alpine grasslands on aerial imagery with a U-Net convolutional neural network. *Remote Sens.* 12 (24), 4149.
- Shapiro, S.S., Wilk, M.B., 1965. An analysis of variance test for normality (complete samples). *Biometrika* 52 (3–4), 591–611.
- Shruthi, R.B., Kerle, N., Jetten, V., Abdellah, L., Machmach, I., 2015. Quantifying temporal changes in gully erosion areas with object oriented analysis. *Catena* 128, 262–277.
- Soman, H., Kizha, A.R., Muñoz Delgado, B., Kenefic, L.S., Kanoti, K., 2020. Production economics: comparing hybrid tree-length with whole-tree harvesting methods. *Forestry: Int. J. Financ. Res.* 93 (3), 389–400.
- Sun, Y., Hao, Z., Guo, Z., Liu, Z., Huang, J., 2023. Detection and mapping of chestnut using deep learning from high-resolution UAV-based RGB imagery. *Remote Sens.* 15 (20), 4923.
- Walpole, R.E., Myers, R.H., Myers, S.L., Ye, K., 2012. Probability and Statistics for Engineering and Science. Pearson Education, pp. 430–435.
- Watts, F.C., Collins, M.E., 2008. Soils of Florida. ASA-CSSA-SSSA.
- Web Soil Survey, 2019. Soil Survey Staff, Natural Resources Conservation Service. United States Department of Agriculture. Retrieved February 10, 2024 from Web Soil Survey. Available online at: <https://websoilsurvey.nrcs.usda.gov/>.
- Wischmeier, W.H., Smith, D.D., 1978. Predicting Rainfall Erosion Losses: a Guide to Conservation Planning. Department of Agriculture, Science and Education Administration.
- Yang, M., Mou, Y., Liu, S., Meng, Y., Liu, Z., Li, P., Xiang, W., Zhou, X., Peng, C., 2022. Detecting and mapping tree crowns based on convolutional neural network and Google Earth images. *Int. J. Appl. Earth Obs. Geoinf.* 108, 102764.
- Yuan, Q., Shen, H., Li, T., Li, Z., Li, S., Jiang, Y., Xu, H., Tan, W., Yang, Q., Wang, J., Gao, J., Zhang, L., 2020. Deep learning in environmental remote sensing: achievements and challenges. *Remote Sens. Environ.* 241, 111716. <https://doi.org/10.1016/j.rse.2020.111716>.
- Zerihun, M., Mohammedyasin, M.S., Sewnet, D., Adem, A.A., Lakew, M., 2018. Assessment of soil erosion using RUSLE, GIS and remote sensing in NW Ethiopia. *Geoderma Regional* 12, 83–90. <https://doi.org/10.1016/j.geodrs.2018.01.002>.
- Zhao, Z., Alzubaidi, L., Zhang, J., Duan, Y., Gu, Y., 2024. A comparison review of transfer learning and self-supervised learning: definitions, applications, advantages and limitations. *Expert Syst. Appl.* 242, 122807. <https://doi.org/10.1016/j.eswa.2023.122807>.
- Zingg, A.W., 1940. Degree and length of land slope as it affects soil loss in run-off. *Agric. Engng.* 21, 59–64.